Composition and strain relaxation of $In_xGa_{1-x}N$ graded core shell-nanorods

Q Y Soundararajah[1], R F Webster[2], I J Griffiths[3], S V Novikov[4] and C T Foxon[4], D Cherns[1]
[1] H H Wills Physics Laboratory, University of Bristol, Tyndall Avenue, Bristol, BS8 1TL, UK
[2] Electron Microscopy Unit, University of New South Wales, Sydney, NSW 2052, Australia
[3] Department of Materials, University of Oxford, Parks Road, Oxford, OX1 3PH, UK
[4] School of Physics and Astronomy, University of Nottingham, Nottingham NG7 2RD, UK

Two $In_xGa_{1-x}N$ nanorod samples with graded In compositions of x = 0.5 - 0 (Ga-rich) and x = 0.5 - 1 (In-rich) grown by molecular beam epitaxy were studied using transmission electron microscopy. The nanorods had wurtzite crystal structure with growth along [0001] and core-shell structures with In-rich core and Ga-rich shell. Energy-dispersive X-ray analysis confirmed grading over the entire compositional range and showed that the axial growth rate was primarily determined by the In flux, and the radial growth rate by the Ga flux. There was no evidence of misfit dislocations due to grading, but the strain due to the lattice mismatch between the In-rich core and Ga-rich shell was relaxed by edge dislocations at the core-shell interface with Burgers vectors $a\langle 11\bar{2}0\rangle$ and $c\langle 0001\rangle$.

Keywords: InGaN nanorods, transmission electron microscopy, EDX mapping, core-shell structures, strain

I. Introduction

The great success of making III-nitrides optoelectronic devices in the blue range has led to interest in extending devices to longer wavelengths for light emitting diodes and lasers working in the green range [1]–[4], and for solar cell applications [5]. $In_xGa_{1-x}N$ has a direct band gap, the energy of which may be varied [6] by changing the In content (x). However the growth of high quality $In_xGa_{1-x}N$ with high In-content is difficult as the lattice mismatch between InN and GaN is 11%, therefore growth of $In_xGa_{1-x}N$ with high In-content on a GaN base introduces dislocations and strain fields [7]. These defects are generally charged and can act as non-radiative recombination centres, a detrimental quality for LED and photovoltaic devices. Strain generated by lattice mismatch between two compositions induces piezoelectric polarization and high electric fields which leads to carrier separation and a reduced recombination efficiency in light emitting devices [8]. Furthermore, InN requires a low growth temperature (compared to GaN) at around 400-500 ℃ due to its higher volatility at elevated growth temperatures that leads to spinodal decomposition and In clustering.

These challenges are potentially resolved in the growth of $In_xGa_{1-x}N$ nanorods by molecular beam epitaxy (MBE). The MBE allows low temperature growth with precise control over the growth parameters that enables more efficient In incorporation. The geometry of the nanorods should also allow misfit strain arising from lattice mismatch with the substrate to be accommodated by permitting elastic relaxation at the lateral free surfaces [9], [10]. The growth of $In_xGa_{1-x}N$ nanorods under N-rich conditions has been studied for over a decade [11] and growth of nanorods over the whole compositional range of x = 0 - 1 has also been demonstrated [12]. The spontaneous growth of core-shell nanorod structures is commonly reported for

$In_xGa_{1-x}N$ and $Al_xIn_{1-x}N$ nanorods grown both by MBE and Magnetron Sputtering techniques [13]–[16]. However, composition grading has been studied less intensively, and the investigation of graded nanorods that cover the entire range of composition was introduced for the first time by our group [17]. Such structures offer potential substrates for high quality $In_xGa_{1-x}N$ overlayers across the composition range [18], as well as a means to achieve wavelength tunable nanorod devices for light emitting diode or solar cell applications [19]. Two $In_xGa_{1-x}N$ samples graded to cover the entire compositional range of x = 0 - 1 grown by plasma-assisted MBE (PA-MBE) are studied in this paper and the compositional and structural changes during grading are analysed.

II. Experiment

Graded $In_xGa_{1-x}N$ nanorods with x = 0.5 - 0 and x = 0.5 - 1 were grown directly on p-type Si(111) substrates under strong N-rich condition for five hours in a Varian ModGen II MBE system. Activated Nitrogen was supplied by HD25 RF plasma source. The samples were grown at ~450 ℃ with the In and Ga sources inclined at ~35° normal to the substrate which was rotated at 10 rpm. The growth process has been started by growing a uniform composition of x = 0.5 for the first three hours followed by a stepwise grading of In/Ga for two hours by just changing Ga/In beam pressures as shown in Table 1. Cross sectional TEM samples were prepared by mechanical polishing followed by Ar^+ beam thinning or by scraping off the nanorods into ethanol and drop-cast onto holey carbon films. The nanorods were studied in cross-sectional orientation (with the growth axis nearly perpendicular to the beam) and in plan-view orientation (growth axis parallel to the beam) by JEOL 2010 and ARM 200F transmission electron microscopes operated at 160 kV and 200 kV respectively. The composition and strain relaxation of the nanorods were studied using EDX and selected area electron diffraction methods.

Table 1: The Ga and In beam equivalent pressure sequence for the two $In_xGa_{1-x}N$ samples.

$In_xGa_{1-x}N$ graded from x=0.5-0 (Ga-rich)		**$In_xGa_{1-x}N$ graded from x=0.5-1 (In-rich)**		**Time duration (hours)**
In BEP (Torr)	**Ga BEP (Torr)**	**In BEP (Torr)**	**Ga BEP (Torr)**	
~3.0 10^{-8}	~2.2 10^{-8}	~3.0 10^{-8}	~2.2 10^{-8}	3
~2.25 10^{-8}	~2.2 10^{-8}	~3.0 10^{-8}	~1.65 10^{-8}	0.5
~1.5 10^{-8}	~2.2 10^{-8}	~3.0 10^{-8}	~1.1 10^{-8}	0.5
~0.75 10^{-8}	~2.2 10^{-8}	~3.0 10^{-8}	~0.55 10^{-8}	0.5
~0	~2.2 10^{-8}	~3.0 10^{-8}	~0	0.5

III. Results and discussion

Nanorods of both graded samples have wurtzite structure with growth along [0001]; the cross sectional TEM images and corresponding selected area electron diffraction (SAED) patterns taken close to the $[11\bar{2}0]$ zone axis using JEOL 2010 TEM are shown in Figure 1. The Ga-rich nanorods are about 700 ± 100 nm long and 100 ± 20 nm wide and the In-rich nanorods are about 1000 ± 200 nm long and 60 ± 20 nm wide. Examination on the nanorods under two beam conditions showed bend contours as well as finer contrast features which will be discussed below.

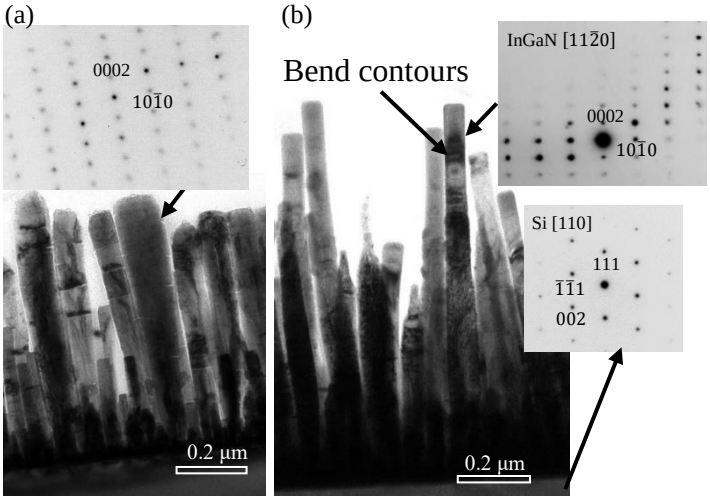

Figure 1: TEM images of ion-thinned cross-sectional specimens showing (a) Ga-rich and (b) In-rich graded samples and the corresponding SAED patterns taken close to $[11\bar{2}0]$ zone axis using JEOL 2010 TEM.

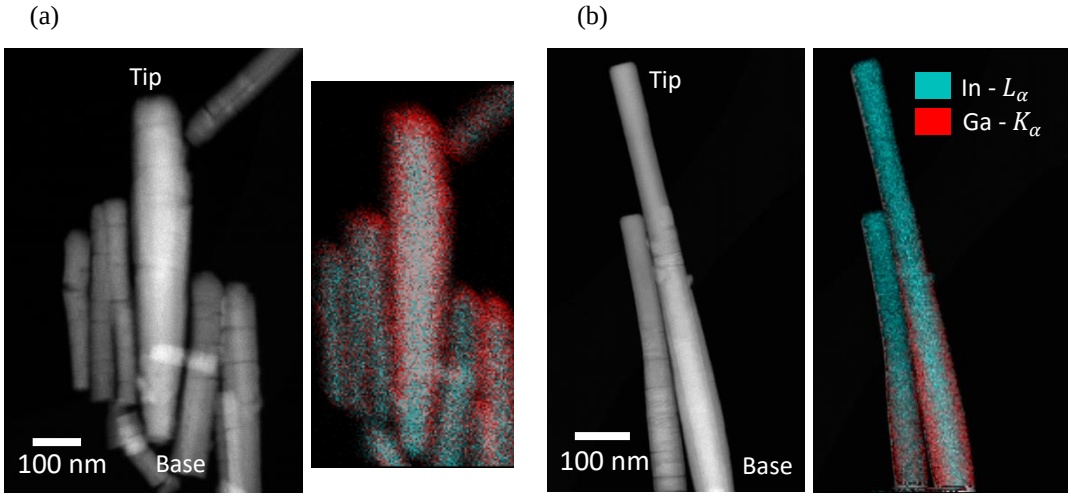

Figure 2: HAADF images and EDX elemental maps of scraped off $In_xGa_{1-x}N$ nanorods with (a) x = 0.5 - 0 and (b) x = 0.5 - 1.

Figure 2 shows high angle annular dark field (HAADF) images and energy dispersive X-ray (EDX) elemental maps taken using the ARM 200F operating at 200 kV equipped with a 100 mm^2 windowless EDX detector. The EDX mapping confirmed the core-shell structure, with In-rich core and Ga-rich shell in the nanorods as previously reported for nanorods grown with a nominal composition of x = 0.5 [13], [17]. Figure 2a shows that the Ga-rich sample has an In-rich core which tapers towards the very end of growth with an increase in thickness of the

Ga-rich shell (Fig. 2a). In contrast, figure 2b has a Ga-rich shell which tapers along the growth direction with no significant changes in the In-rich core thickness observed. Moreover, the Ga-rich nanorods are both shorter and broader than the In-rich nanorods. Both samples show no evidence of abrupt composition changes corresponding to the discrete steps in beam pressures during growth (Table 1). This suggests some significant diffusion of both Ga and In adatoms on the growth surfaces to enhance composition gradients in the growth direction.

Figure 3 shows EDX line scans along the growth direction for scraped off nanorods from both samples. Figure 3 (a) shows the grading to GaN (x = 0.5 to 0). The composition of this rod is about x = 0.5 which is constant until the final 100 nm of growth. Given that the average nanorod length for this sample was around 700 ± 100 nm from standard cross-sectional samples (as in Figure 1), this suggests that the initial 3 hrs of growth corresponds to a nanorod length of approximately 600 nm, consistent with previous studies on nominal x = 0.5 nanorods [13], and the final two hours of graded growth (x = 0.5 - 0) corresponds to a length of only 100 nm. The Ga-rich graded sample, therefore, has a growth rate of about 200 nm hr^{-1} which is then reduced to an average of 50 nm hr^{-1} for the graded growth. This shows that the growth rate along [0001] direction is primarily dependent on the In pressure which reduces during grading while the Ga pressure remains constant.

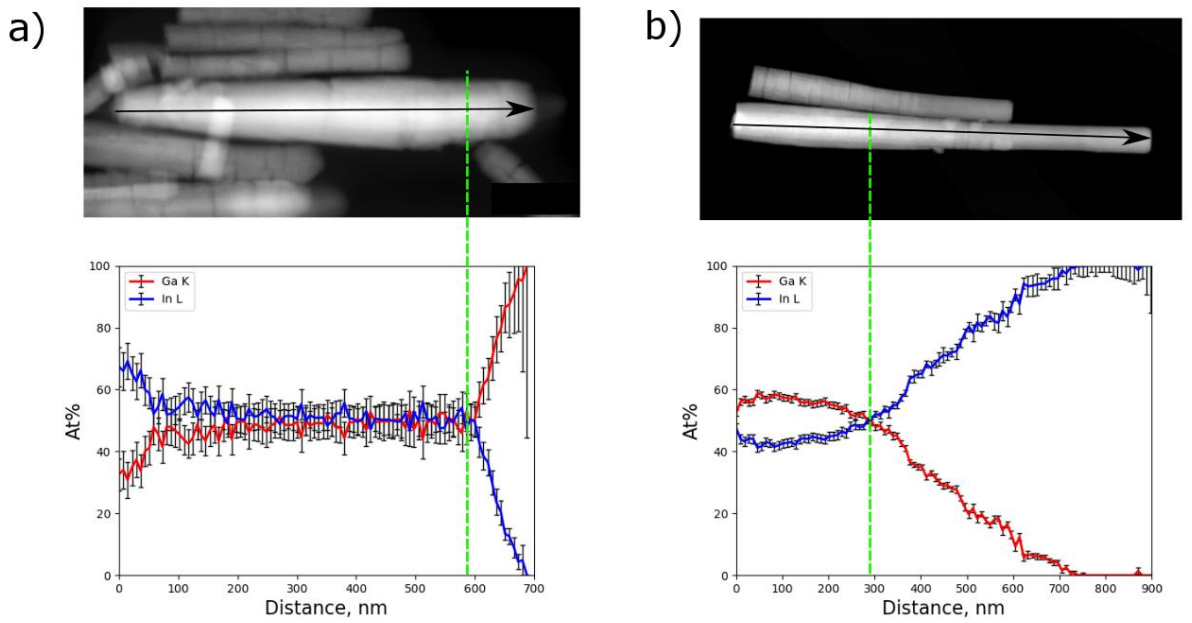

Figure 3: HAADF-STEM images and the elemental EDX line scans of Ga-K and In-L taken along the indicated arrows in the images and (a, c) Ga-rich and (b, d) In-rich graded $In_xGa_{1-x}N$ nanorods scraped off from the substrate. The distance is measured in the growth direction, from the start of the arrows indicated in (a) and (b). Dotted lines indicate the approximate point where the composition starts to vary due to grading.

The In-rich graded sample (x = 0.5 - 1), in figure 3 (b) on the other hand shows a gradual increase of In content along the growth direction from the dotted line. The average growth rate along the [0001] direction during grading was about 230 nm hr^{-1} from cross-sectional samples, but is slightly greater for the nanorod in Figure 3b (about 300 nm hr^{-1}), not unexpected from the natural variation (Figure 1). This is greater than that during the first 3 hours of x = 0.5

growth (200 nm hr^{-1}). This again suggests that this axial growth rate is controlled by the In flux which was constant throughout growth and not by the Ga flux which was decreased during grading. The increased In concentration in the core compared to the expected composition (x = 0.5) suggests that In diffusion from the sidewalls to the (0001) surface during growth is a significant factor. The increase in the axial growth rate during grading may indicate that this contribution is enhanced, suggesting that the Ga adatom flux plays a role in binding In to the sidewalls. However, given the variability in the growth rate, the results are not conclusive on this point.

The tapering of the shell in the In-rich sample shows that the lateral growth is reduced as the Ga flux is decreased consistent with the assumption that all the Ga adatoms arriving on the side walls are absorbed with low diffusion or re-evaporation rates, and that lateral growth is much less sensitive to the In flux. This also implies that the nanorod radius should be roughly constant for the Ga-rich samples where the Ga flux stays the same while the In flux is reduced. This is also consistent with the observations in figures 1 and 2.

From the elemental EDX mapping of the In-rich sample, the compositions in the core and shell during the first 3 hours of growth were determined to be $x = 0.68 \pm 0.04$ and $x = 0.34 \pm 0.02$ respectively, corresponding to a difference in lattice parameters between the core and shell of about 0.012 ± 0.002 nm equivalent to a lattice misfit of 0.04 ± 0.005. If the core-shell interface is coherent (matched in-plane lattice parameter), the core should be under isotropic compression. On the other hand the Ga-rich shell is under compensative tensile stress along the c axis and is free to relax in all other directions. In such geometries, strain energy should be reduced and relaxed when the core radii and the shell thickness exceed the critical thickness, by forming dislocations, or by surface roughening. The critical core radii and the shell thickness are previously reported for various InGaN core-shell nanorod structures [20] where the critical shell thickness is dependent on the core radius. During the first 3 hours of growth, the In-rich graded sample has core radii about 50 ± 10 nm and shell thickness about 25 ± 5 nm and the Ga-rich sample has core radii about 65 ± 5 nm and shell thickness about 30 ± 10 nm which exceed the critical core radii and shell thickness which should be < 10 nm [21]. The surfaces are smooth and therefore it is expected that the samples of this study should have dislocations produced to accommodate the lattice mismatch. This was investigated firstly by selected area electron diffraction (SAED) using both $[10\bar{1}0]$ and $[0002]$ systematic rows of reflections using a long camera length (50 and 80 cm calibrated with Si substrate) with an area of illumination ~125 nm covered by the SAED aperture.

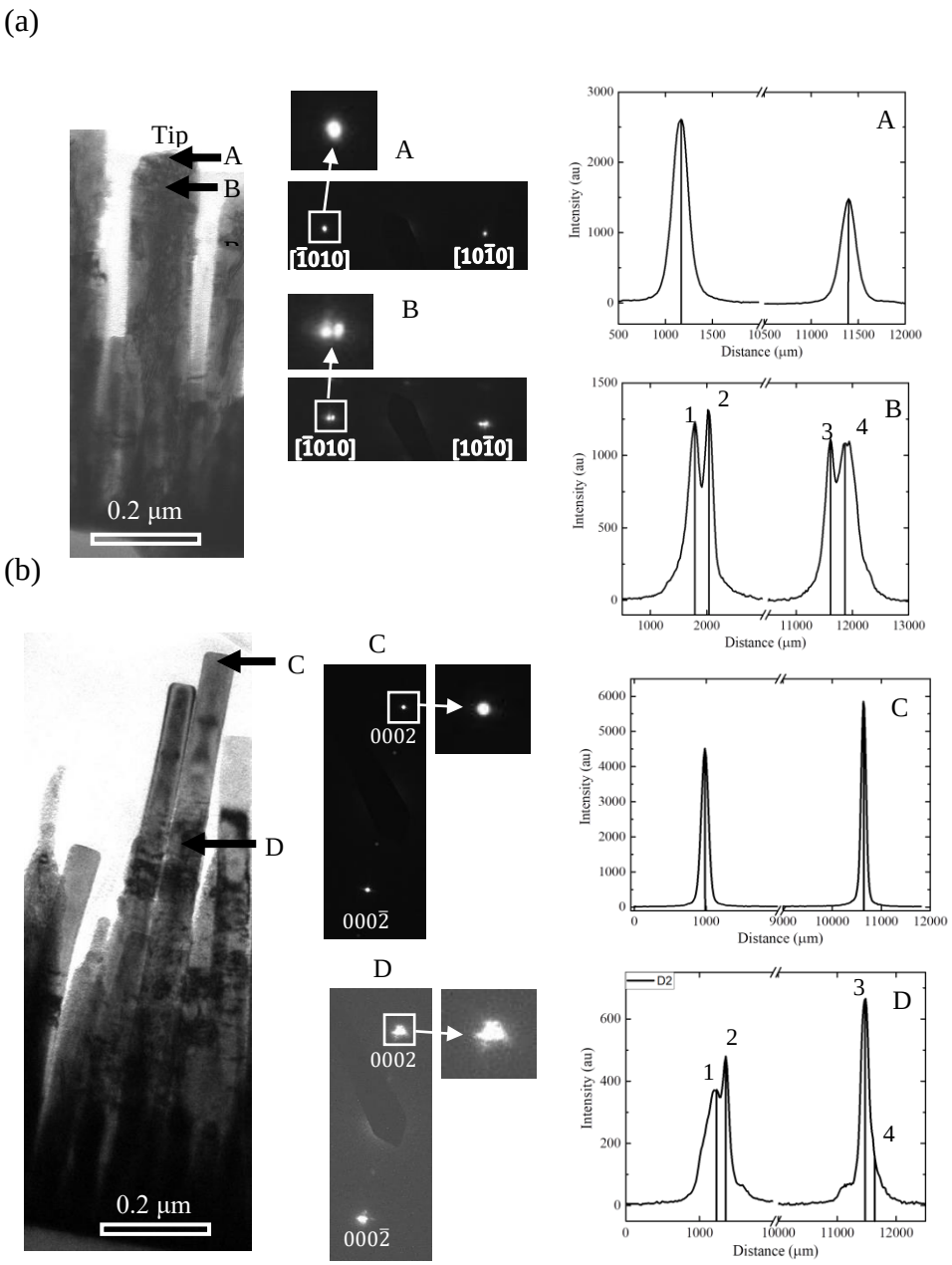

Figure 4: SAED patterns showed splitting of both the [10$\bar{1}$0] and [0002] reflections due to the core-shell structure. This figure illustrates SAED patterns (centre beam blanked out) from cross-sectional samples and the corresponding intensity line profiles for (a) the [10$\bar{1}$0] systematic row (Ga-rich graded sample) and (b) the [0002] systematic row (In-rich graded sample). The peak positions are indicated by vertical lines.

The SAED patterns taken on the graded rods show split spots (labelled by B and D in figure 4) in both directions along [10$\bar{1}$0] and [0002] below the tip of the rods indicating a lattice mismatch between the core and shell. There are single sharp spots only at the tip (labelled by A and C) consistent with the single composition. The lattice parameter estimations using [0002] and [10$\bar{1}$0] systematic rows reflections, along the growth direction of the rods are plotted below in figures 5 for the Ga-rich and In-rich samples. The onsets of the graded regions are indicated by dotted lines.

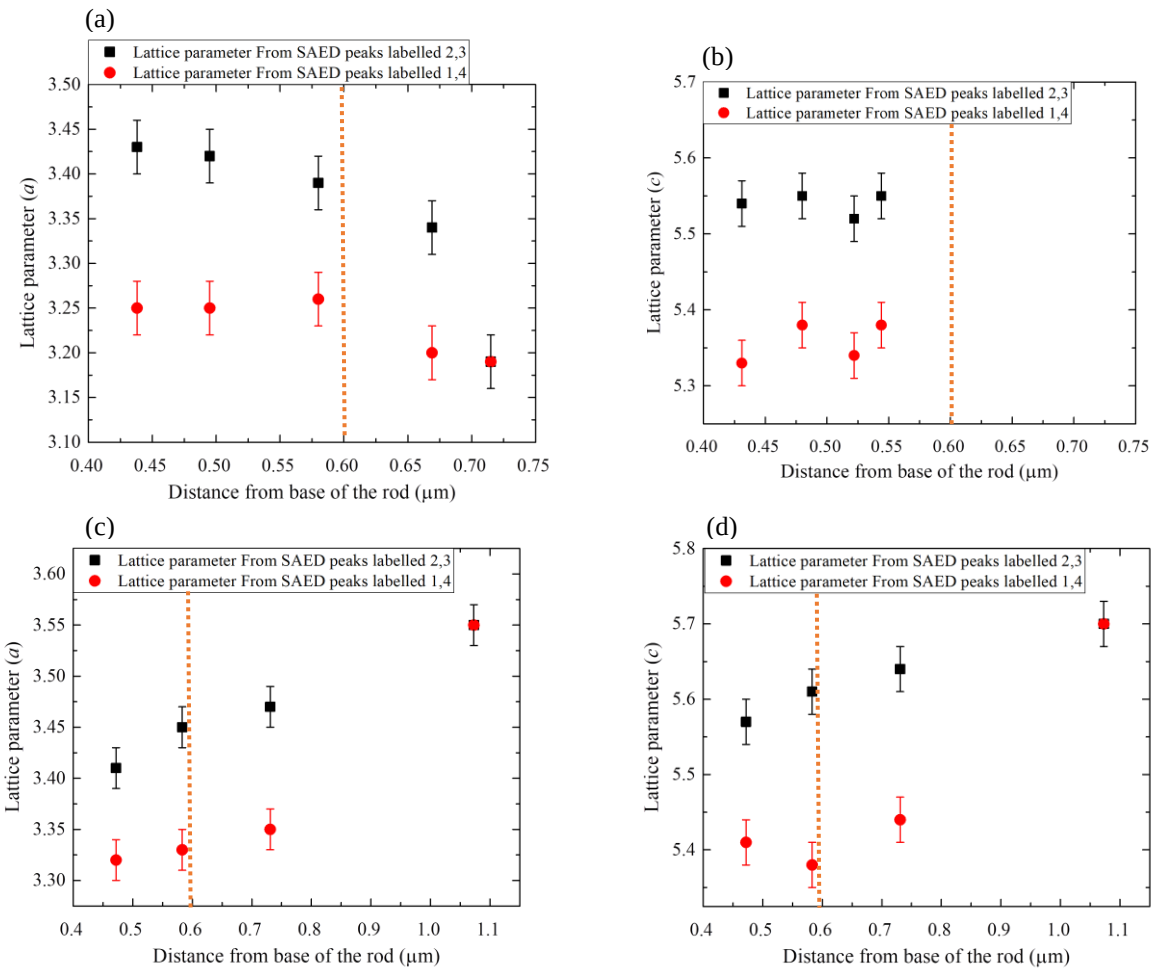

Figure 5: (a, b) Ga-rich graded sample and (c, d) In-rich graded sample: Lattice parameters calculated using (a, c) $[10\bar{1}0]$ and (b, d) [0002] systematic rows reflections. The dotted lines mark the approximate points at which grading begins.

The inner spots specified by 2 and 3 in the intensity profiles in fig. 4 correspond to the In-rich (core) region and the outer spots (specified by 1 and 4) to the Ga-rich (shell) region. The lattice parameters generally decrease with growth for Ga-rich samples and increase with growth for In-rich samples consistent with the grading. We expect that the system will be fully relaxed if the estimated mismatch from Figure 5 is equal to the equilibrium lattice mismatch calculated for the core and shell compositions from the EDX data, and is partially relaxed when it is less than that [9], [10]. From Figure 5, the average lattice misfit between core and shell for the In-rich graded nanorods during the first 3 hours of growth appears constant within the experimental error, and was calculated to be ~0.030 ± 0.005 along $[10\bar{1}0]$ and [0002] directions. The corresponding misfits for Ga-rich graded nanorods were calculated to be 0.05 ± 0.01 along $[10\bar{1}0]$ and 0.032 ± 0.006 along [0002]. The mismatch for fully-relaxed lattices is estimated from the measured compositions to be about 4% along both directions suggesting that there is a near-complete strain relaxation along both $[10\bar{1}0]$ and [0002] directions in the two graded samples.

Figure 6 shows a bright field image of an In-rich nanorod taken using JEOL 2010 TEM with $\{0002\}$ systematic row reflections operating. It shows periodic contrast features, as arrowed in the inset, which would be consistent with a set of edge dislocations at the core-shell interface that has a periodicity of 11-13 nm. If we assume these are edge dislocation loops lying in the shell around the core diameter with Burgers vector $c[0001]$, the spacing between the dislocation cores corresponds to a misfit of 4 ± 1%, consistent with full relaxation of mismatch strain in the c-direction.

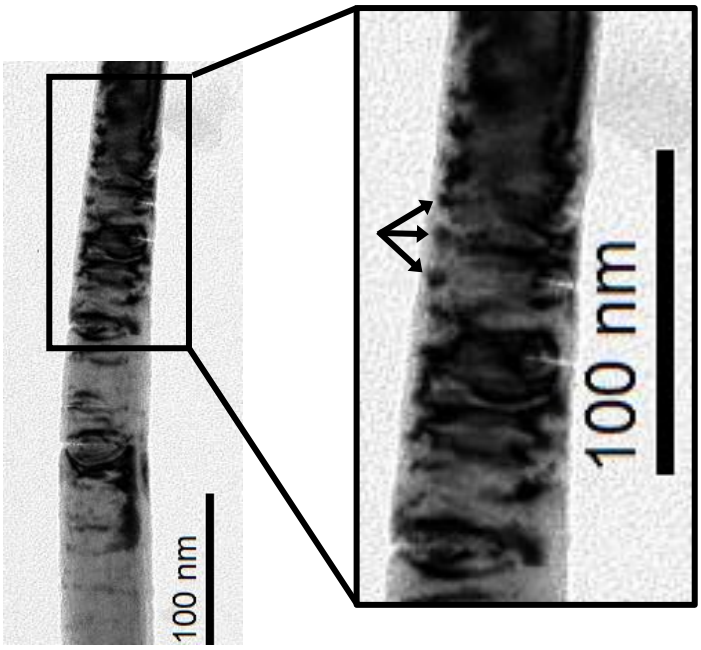

Figure 6: Bright field TEM images of an In-rich graded sample taken at [0002] systematic row with a section magnified in the inset that shows dislocation cores and Moiré fringes.

The general contrast across the central region of the nanorod in Figure 6 is relatively complicated, but can be partially described as moiré fringes. These arise owing to the overlap of the misfitting core and shell lattices. The spacing of the Moiré fringes (D) can be related to the d-spacings of the two lattices [9], [10] through $D = \frac{d_1 d_2}{(d_1 - d_2)}$ where d_1 and d_2 refer to the main diffracting planes for the core and shell which are the (0002) planes. The spacing of Moiré fringes observed in this region is approximately D = 6.3 nm, i.e. around half the dislocation spacing, giving a misfit of 4.4 ± 0.4%, consistent with the equilibrium misfit of 4.0 ± 0.5% estimated earlier from the EDX data.

Misfit dislocations running parallel to the nanorod axis can be seen in plan-view cross sections. A high resolution HAADF image of an ungraded plan view sample of x = 0.5 taken at the core-shell interface is shown in figure 7. The Bragg filtered image using $[10\bar{1}0]$ reflections shows that there are edge-on dislocations at the core-shell interface with a spacing of about 5 nm. These dislocations have Burgers vector $a[11\bar{2}0]$as seen in the Burgers circuit. The spacing between the dislocation cores corresponds to 15 lattice planes that has a misfit of 6 ± 1%, which is comparable to the misfit of the relaxed lattice which is about 4%.

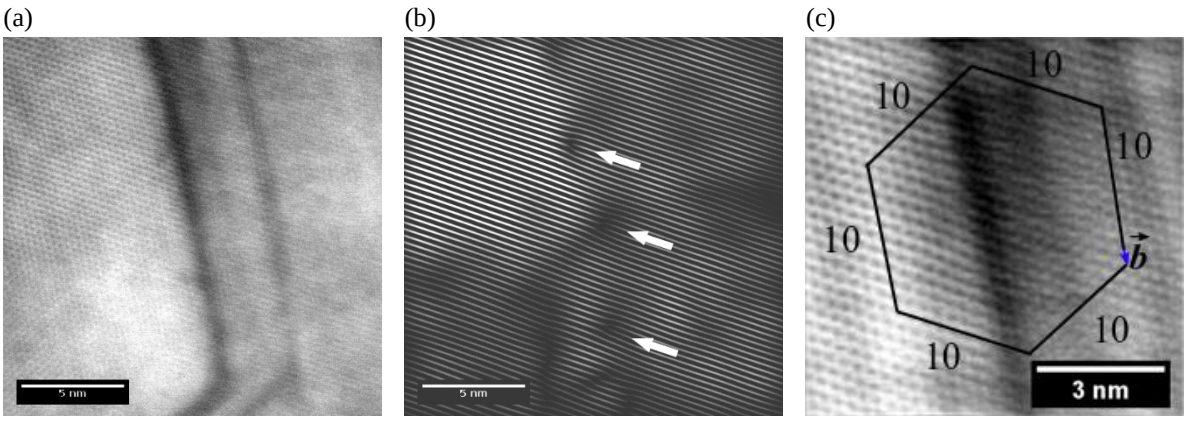

Figure 7: (a) HAADF image of a core-shell interface of a plan-view cross section, (b) Bragg filtered image of (a) using $g = 10\bar{1}0$ reflections and the edge dislocation cores are indicated by white arrows. (c) a Burgers circuit used to characterise the dislocation type and the blue arrow indicates the Burgers vector is to be $\langle 11\bar{2}0 \rangle$.

Thus the results in Figures 6 and 7 clearly show that the line and loop edge dislocations are formed to relieve the radial and axial strain in the nanorods due to the core-shell geometry.

IV. Conclusions

The $In_xGa_{1-x}N$ graded samples which were grown by PA-MBE under N rich condition have nanorods with single crystalline hexagonal wurtzite structure grown along [0001] direction. These nanorods intrinsically grow with core-shell structures with In-rich core and Ga-rich shell. The entire range of composition of x = 0 - 1 has been achieved by grading and confirmed by the EDX analysis. The growth rates and the aspect ratio of the nanorods strongly depend on their composition. The In-rich sample demonstrates a higher axial growth rate with taller and tapering nanorods and the Ga-rich sample shows a higher radial growth rate with relatively larger diameters. From the measured growth rates, the results suggest strongly that the axial growth rate is controlled by the In flux and the radial growth rate by the Ga flux.

The core-shell structures are also manifested in the SAED patterns by the splitting of diffraction spots observed along both the [0001] and $[10\bar{1}0]$ directions. The mismatches between the diffraction spots agree with the equilibrium lattice mismatches estimated from the measured core and shell compositions both in the radial and axial direction, suggesting a near-complete strain relaxation occurs in the nanorods. There is evidence for misfit dislocations with Burgers vector $c[0001]$ present as loops surrounding the core and edge dislocations with Burgers vector $a < 11\bar{2}0 >$ which run parallel to the nanorod axis but confined at the core-shell interface. Although there may be potential benefits of the core-shell structure for nanorod devices, e.g. carriers should be confined to the (lower bandgap) In-rich core and away from surface traps, it is possible that these misfit dislocations act as non-radiative recombination centres at the core-shell interface instead! In contrast, no threading dislocations were observed other than those at the core-shell interface, indicating that the single crystal InN and GaN regions at the nanorod tips were defect-free, suggesting that these graded nanorods could provide substrates for high quality InN- or GaN-based devices [18].

Acknowledgments

The authors are grateful for the funding for the growth of nanorods under EPSRC grant EP/I035501/1, and for the use of the JEOL ARM 200F, South of England Analytical Electron Microscope under EPSRC grant EP/K040375/1.

References

[1] M. H. Crawford, "LEDs for solid-state lighting: Performance challenges and recent advances," *IEEE J. Sel. Top. Quantum Electron.*, vol. 15, no. 4, pp. 1028–1040, 2009.

[2] S. Pimputkar, J. S. Speck, S. P. Denbaars, and S. Nakamura, "Prospects for LED lighting," *Nat. Photonics*, vol. 3, pp. 180–182, 2009.

[3] Y. Jiang, Y. Li, Y. Li, Z. Deng, T. Lu, Z. Ma, P. Zuo, L. Dai, L. Wang, H. Jia, W. Wang, J. Zhou, and W. Liu, "Realization of high-luminous- efficiency InGaN light-emitting diodes in the ' green gap ' range," *Nat. Publ. Gr.*, vol. 14, pp. 1–7, 2015.

[4] M. Royo, M. De Luca, R. Rurali, X. Zhang, H. Lourenço-martins, S. Meuret, and M. Kociak, "InGaN nanowires with high InN molar fraction: growth, structural and optical properties," *Nanotechnology*, vol. 27, p. 195704, 2016.

[5] J. Wu, W. Walukiewicz, K. M. Yu, W. Shan, J. W. Ager, E. E. Haller, H. Lu, W. J. Schaff, W. K. Metzger, and S. Kurtz, "Superior radiation resistance of In1-xGaxN alloys: Full-solar-spectrum photovoltaic material system," *J. Appl. Phys.*, vol. 94, no. 10, pp. 6477–6482, 2003.

[6] A. G. Bhuiyan, K. Sugita, A. Hashimoto, and A. Yamamoto, "InGaN solar cells: Present state of the art and important challenges," *IEEE J. Photovoltaics*, vol. 2, no. 3, pp. 276–293, 2012.

[7] T. Takeuchi, S. Sota, M. Katsuragawa, M. Komori, H. Takeuchi, H. Amano, and I. Akasaki, "Quantum-Confined Stark Effect due to Piezoelectric Fields in GaInN Strained Quantum Wells," *Jpn. J. Appl. Phys.*, vol. 36, pp. L382–L385, 1997.

[8] E. T. Yu, X. Z. Dang, P. M. Asbeck, S. S. Lau, and G. J. Sullivan, "Spontaneous and piezoelectric polarization effects in III–V nitride heterostructures," *J. Vac. Sci. Technol. B Microelectron. Nanom. Struct.*, vol. 17, no. 4, pp. 1742–1749, 1999.

[9] R. Popovitz-biro, A. Kretinin, P. Von Huth, and H. Shtrikman, "InAs/GaAs Core-Shell Nanowires," *Cryst. Growth Des.*, vol. 11, pp. 3858–3865, 2011.

[10] K. L. Kavanagh, I. Saveliev, M. Blumin, G. Swadener, and H. E. Ruda, "Faster radial strain relaxation in InAs – GaAs core – shell heterowires," *J. Appl. Phys.*, vol. 111, no. 4, 2012.

[11] E. Calleja, J. Ristić, S. Fernández-Garrido, L. Cerutti, M. a. Sánchez-García, J. Grandal, A. Trampert, U. Jahn, G. Sánchez, A. Griol, and B. Sánchez, "Growth, morphology, and structural properties of group-III-nitride nanocolumns and nanodisks," *phys. stat. sol*, vol. 244, no. 8, pp. 2816–2837, 2007.

[12] T. Kuykendall, P. Ulrich, S. Aloni, and P. Yang, "Complete composition tunability of InGaN nanowires using a combinatorial approach," *Nat. Mater.*, vol. 6, no. 12, pp. 951–956, 2007.

[13] D. Cherns, R. F. Webster, S. V Novikov, C. T. Foxon, a M. Fischer, F. a Ponce, and S. J. Haigh, "Compositional variations in In0.5Ga0.5N nanorods grown by molecular beam epitaxy," *Nanotechnology*, vol. 25, p. 215705, 2014.

[14] M. Gómez-Gómez, N. Garro, J. Segura-Ruiz, G. Martinez-Criado, A. Cantarero, H. T. Mengistu, A. García-Cristóbal, S. Murcia-Mascarós, C. Denker, J. Malindretos, and A.

Rizzi, “Spontaneous core-shell elemental distribution in In-rich InxGa1-xN nanowires grown by molecular beam epitaxy,” *Nanotechnology*, vol. 25, p. 075705, 2014.
[15] E. A. Serban, P. O. Åke Persson, I. Poenaru, M. Junaid, L. Hultman, J. Birch, and C.-L. Hsiao, “Structural and compositional evolutions of InxAl1-xN core–shell nanorods grown on Si(111) substrates by reactive magnetron sputter epitaxy,” *Nanotechnology*, vol. 26, p. 215602, 2015.
[16] J. Segura-Ruiz, G. Martínez-Criado, C. Denker, J. Malindretos, and A. Rizzi, “Phase separation in single InxGa1-xN nanowires revealed through a hard x-ray synchrotron nanoprobe,” *Nano Lett.*, vol. 14, no. 3, pp. 1300–1305, 2014.
[17] R. F. Webster, Q. Y. Soundararajah, I. J. Griffiths, D. Cherns, S. V Novikov, and C. T. Foxon, “Microstructure of InxGa1− xN nanorods grown by molecular beam epitaxy,” *Semicond. Sci. Technol.*, vol. 30, no. 11, p. 114014, 2015.
[18] D. Cherns, R. F. Webster, S. V Novikov, C. T. Foxon, A. M. Fischer, and F. A. Ponce, “The growth of In 0 . 5 Ga 0 . 5 N and InN layers on (1 1 1) Si using nanorod intermediate arrays,” *J. Cryst. Growth*, vol. 384, pp. 55–60, 2013.
[19] T. R. Kuykendall, A. M. Schwartzberg, and S. Aloni, “Gallium Nitride Nanowires and Heterostructures: Toward Color-Tunable and White-Light Sources,” *Adv. Mater.*, vol. 27, no. 38, pp. 5805–5812, 2015.
[20] S. Raychaudhuri and E. T. Yu, “Critical dimensions in coherently strained coaxial nanowire heterostructures,” *J. Appl. Phys.*, vol. 99, p. 114308, 2006.
[21] S. Raychaudhuri and E. T. Yu, “Calculation of critical dimensions for wurtzite and cubic zinc blende coaxial nanowire heterostructures,” *J. Vac. Sci. Technol. B*, vol. 24, no. 4, pp. 2053–2059, 2006.